scientific reports

Check for updates

OPEN

Cancer cells impact the microrheology of endothelial cells during physical contact or through paracrine signalling

Georgia M. Kefala[1,2], Daria Tsvirkun[1], Valérie M. Laurent[1] & Claude Verdier[1✉]

During the process of metastasis, cancer cells transmigrate through the endothelial barrier of the vascular walls. Cancer cells interact with the endothelial cells, leading to changes of their mechanical properties. While this interaction has been extensively studied from the perspective of cancer cells (CCs), the mechanical properties of the endothelium remain underexplored, even though they may play a crucial role in regulating this process. In this study, we used a microrheology AFM-based approach to demonstrate that the properties of endothelial cells (ECs) are altered when cultured either in CC-conditioned medium or in direct contact with cancer cells. We found that the viscoelasticity of ECs decreased when cultured in diluted CC-conditioned medium. Furthermore, ECs in direct contact with a cancer cell at short times (less than 30 min) also showed significantly lower stiffness and viscoelastic moduli. In parallel, we observed a reduction in the quantity of actin fibers and actin clusters within the EC cytoskeleton, resulting in a less structured network that may facilitate CC transmigration. Overall, our findings indicated that the rheological properties of ECs can be altered either directly through physical contact with CCs or indirectly via CC-secreted substances. This suggests that the endothelium actively responds to the presence of cancer cells, rather than serving only as a passive barrier.

Vascular endothelial cells (ECs) line the inner walls of blood vessels and constantly interact with the blood flow and surrounding tissues. The endothelial cell monolayer with adherens junctions and tight junctions provides the functional integrity of blood vessels and forms a selective barrier to control the movement of molecules and cells in and out of the bloodstream[1]. Dysfunction of the endothelial monolayer leads to a variety of cardiovascular and metabolic disorders[2]. Understanding the differences in the mechanical properties of the endothelial monolayer, under normal and abnormal conditions, may provide insight into the pathogenesis of circulatory disorders and diseases. The mechanisms of transendothelial migration have been extensively studied in the case of monocytes[3,4], but such mechanisms are also particularly relevant in the case of cancer metastasis. Upon detaching from a primary tumour, cancer cells (CCs) migrate towards the endothelium, cross it to become circulating cancer cells, and later transmigrate through the endothelium once again to invade secondary tissues[5]. This process remains poorly understood due to its multifactorial and multicomponent nature, involving a complex interplay between cellular biochemical and mechanical signals and their surroundings. In addition, the role of the mechanical properties of endothelial cells has not been extensively studied.

In previous studies, the endothelial monolayer has been viewed as a passive barrier in metastasis and cancer cell migration. However, it is increasingly becoming more evident that endothelial and cancer cells interact in a bidirectional and dynamic manner[6,7]. Initially, these interactions rely on primary adhesive contacts between ECs and CCs, involving molecules such as integrin $\beta 1$[8,9], MUC-1, CD43[10] on the cancer cell side and proteins such as VCAM-1, PECAM-1, and particularly ICAM-1[11,12] on the endothelial side. Many studies have focused on the investigation of cancer cell mechanics. It has been shown that CCs can deform a lot during the transmigration process and are less rigid[13–17]. Cancer cell protrusions may also enable anchoring to the sub-endothelial extracellular matrix (ECM), facilitating subsequent transmigration of CCs[18,19]. Advanced 3D microfluidic platforms, coupled with confocal microscopy[20–22], have been developed to enable precise quantification of

[1]Université Grenoble Alpes, CNRS, LIPhy, Grenoble 38000, France. [2]Leiden University, P.O. Box 9500, 2300 RA Leiden, The Netherlands. ✉email: claude.verdier@univ-grenoble-alpes.fr

endothelial permeability and to estimate the time required for CCs to cross the endothelial barrier (e.g. 4 h in the case of T24 bladder cancer cells[20]).

The actomyosin protein complex is a key component of the endothelial cell cytoskeleton, essential for maintaining endothelial functionality and integrity. However, during interactions between CCs and ECs, VE-cadherins[23,24] and N-cadherins[25] also play a role, particularly in relation to EC contractility. It has also been reported that melanoma cells interact with ECs and use signalling pathways that trigger actinomyosin contractility and disassembly of endothelial cell-cell junctions[26]. Following the recent suggestions that endothelial cells are actively involved in cancer cell transmigration[6], several studies focused on exploring the dynamics of EC mechanical properties under different conditions. The elastic modulus of endothelial cells, typically in the range of 1–5 kPa, is primarily influenced by actin microstructures rather than microtubules[27]. The elastic modulus increases with the development of cell-cell contacts[28] and with loading rate[29], although ECs can also exhibit mechanical heterogeneity at the nanoscale[30]. Mierke[31] showed that endothelial cells in co-culture have an impact on the invasiveness of breast cancer cells, while the stiffness of ECs is reduced by remodeling of their actin cytoskeleton. Javanmardi et al.[19] also underlined the important role of the endothelial actomyosin complex contractility. Finally, viscoelastic responses of ECs were reported, particularly in lamellipodium dynamics, showing a decreased rigidity and increased liquid-like behaviour during gap closure[32].

Experimentally, it has been observed that in co-culture, endothelial cells actively extend toward cancer cells, rather than the reverse[7]. However, the presence of cancer cells can affect the behaviour and mechanical response of the endothelial cells, not only by direct physical contact[11] but also through paracrine signalling[7]. Cancer cells secrete various substances, including growth factors, enzymes, and proteins[33], activating chemical and mechanical signalling pathways in nearby cells and tissues[34]. Recently, it was shown that tumour cells-derived exosomes (extracellular vesicles, 30–150 nm in diameter) facilitate transendothelial migration of breast cancer cells by downregulating the expression of intracellular contact molecules in ECs, thereby disrupting their intercellular integrity[35]. Finally, inflammatory stimuli[36] could induce Endothelial to Mesenchymal Transition (EndMT) of ECs, causing alterations in endothelial functions, which may contribute to the pathogenesis of various diseases. On the other hand, tumour progression and metastasis are known to be associated with inflammation and secretion of diverse cytokines by the tumour microenvironment[37,38].

These studies highlight the importance of understanding the mechanical response of ECs when exposed to an environment altered by CCs or in direct contact with CCs. Here, we used an AFM-based microrheology technique[17,39,40] to study the viscoelastic properties of the endothelium in the presence of paracrine factors secreted by T24 cancer cells or through direct contact with these cells. This technique provides the advantage of obtaining multiple measurements at different timescales within a single experiment. The viscoelastic response of the cell—in particular G^*, the complex shear modulus—varies with the frequency of the applied indentation due to different relaxation times involved[41,42]. At short timescales, the cytoskeleton does not have enough time to reorganize itself, and as a result, the cell appears stiffer, whereas it is softer at longer timescales. During the same experiment, we also measured the Young's modulus of endothelial cells under three experimental conditions: (a) control, (b) in cancer cell conditioned medium, and (c) in contact with cancer cells. A decrease of the EC elastic modulus (E) was found in both studied conditions, when in contact with CCs or in the presence of factors secreted by CCs. The viscoelastic data also exhibited significant differences in both cases, as compared to the control. AFM results were consistent with actin cytoskeleton observations, from confocal microscopy, showing a significant decrease in actin cluster areas.

Results

Endothelial cells cultured in T24-ECGM

To investigate whether the cancer cell can influence the mechanical properties of endothelial cells even in the absence of direct contact and cell–cell interactions, we first focused on studying endothelial monolayers cultured in cancer cell conditioned medium (T24-ECGM). Using the initial approach of the AFM cantilever on the cell (as described in the Methods), the Young's elastic modulus of the cells was calculated from Eq. (1). AFM measurements were performed on ECs cultured in T24-ECGM and on ECs in conventional ECGM, which served as the controls. The median value of the Young's modulus E (Fig. 1a) of the ECs cultured in T24-ECGM was found to be 1.3 kPa (n = 57), whereas for the controls it was 1.8 kPa (n = 43). No significance difference was found between the two data sets ($p = 0.08$).

Using the microrheology technique, during which the AFM cantilever oscillated at frequencies in the range of 2–200 Hz, the elastic G' and viscous G'' moduli were calculated for each frequency using Eq. (2). The averaged data points (n = 43 for controls and n=57 for ECs in T24-ECGM) were plotted as a function of frequency (Fig. 1b), and fitted with two power laws: $G' = G_a\,f^a + G_b\,f^b$ or $G'' = G_c\,f^c + G_d\,f^d$ (f is in Hz, since $f_0 = 1$ Hz in Eq. (3)). The G' curve of ECs cultured in T24-ECGM demonstrated consistently lower values than those of the controls, an indication of the softening of the cells. The fitted curves were compared using the extra-sum-of-squares F test, which showed a low p-value and a high F-value (Table 1), indicating a significant difference between the two G' curves ($p < 0.0001$). For both cases (control and T24-ECGM), the results of fitting (Table 1) showed that the elastic modulus G' had a small slope ($a < 0.1$) for low frequencies and a large one ($b > 2$) for frequencies at the higher end of the range studied. However, ECs cultured in T24-ECGM exhibited larger slopes than the controls (1.28 times larger for exponent a and 1.09 times larger for exponent b). In terms of the viscous modulus G'', we observed that the slope for ECs cultured in T24-ECGM closely approximated that of the control group (Table 1). However, ECs in T24-ECGM curve exhibited quantitatively higher values across the measured frequency range, with the statistical test showing that the curves were significantly different ($p < 0.0001$, F = 508.6 (4,22), Table 1).

Overall, the viscoelastic behaviour in the two cases was similar, as both moduli G' and G'' increased monotonically with the frequency. Additionally, the storage modulus (G') was the dominant component at lower
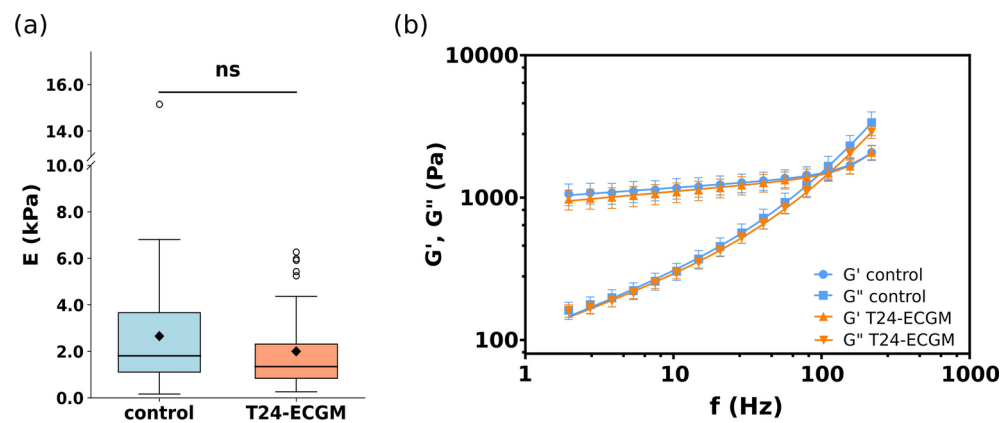
(a)

(b)

Fig. 1. Stiffness and viscoelastic moduli of ECs cultured in T24-ECGM were decreased compared to the controls. (**a**) Boxplot of the Young's modulus E of the controls (blue, n = 43) and ECs cultured in T24-ECGM (orange, n = 57) ($p = 0.08$, Mann–Whitney U test). (**b**) G' and G'' of controls (blue, n = 43) and ECs in T24-ECGM (orange, n = 57) as a function of frequency. Data points correspond to the mean value, while the error bars stand for the SEM. The continuous curves correspond to the best fittings of the data, according to Eq. (3). The fitting parameters are listed in Table 1.

	G_a (Pa)	a	G_b (Pa)	b	R^2	p-value	F-value
G'_{ctrl} (Pa)	988.1	0.07	0.002	2.35	0.998	< 0.0001	29.71 (4, 22)
G' (Pa)	890.2	0.09	0.0006	2.56	0.998		
	G_c (Pa)	c	G_d (Pa)	d	R^2	p-value	F-value
G''_{ctrl} (Pa)	109.1	0.4	1.28	1.4	0.999	< 0.0001	508.6 (4, 22)
G'' (Pa)	109.3	0.38	1.4	1.35	0.999		

Table 1. Fitting parameters of G', G'' and their statistical comparison results (T24-ECGM vs. control).

frequencies, whereas the loss modulus (G'') dominated at higher frequencies. Due to this similar behaviour, as well as the differences described above, the transition frequency f_T, where the elastic modulus equals the viscous modulus ($G' = G''$), was higher for ECs in T24-ECGM (111.1 Hz) as compared to the controls (97.0 Hz). Therefore, ECs exposed to T24-secreted substances showed a delay before the appearance of the glassy regime[17].

Endothelial cells in contact with T24 cancer cells

Given our findings on the mechanical properties of ECs cultured in T24-ECGM, we then investigated whether similar effects would be observed when the ECs are in direct contact with cancer cells. T24 cells were added on confluent EC monolayers and AFM measurements were performed using the microrheology technique. The measurements were performed within the first 30 min after adding the cells and only on ECs found to be in direct contact with a T24 cell. EC monolayers cultured in conventional ECGM served as the controls. In this case (Fig. 2a), the median value of the Young's modulus E for ECs in contact with T24 cells was found to be 0.7 kPa (n = 40), while for the controls it was 1.4 kPa (n = 29). The stiffness of the ECs in contact with T24 cells exhibited a significant decrease as compared to the controls ($p = 0.008$).

When comparing the stiffness of ECs in T24-ECGM medium with ECs in contact with T24s, since controls are different we preferred to study the median value of the ratio $\frac{E}{E_{ctrl}}$. This value was 0.75 for ECs in T24-ECGM medium and 0.51 in the case of contact with T24s, therefore supporting the idea that the effect of contact decreases the elastic modulus more than the medium change ($p < 0.05$).

The elastic G' and viscous G'' moduli, obtained from microrheology measurements, were plotted as a function of frequency (Fig. 2b). The data points correspond to the mean values of ECs moduli in controls (n = 40) or contact experiments with T24 cells (n = 29). As discussed previously, they were fitted using a sum of power-laws: $G' = G_a f^a + G_b f^b$ and $G'' = G_c f^c + G_d f^d$.

By fitting the data sets, we found that the exponent a of G' of ECs in contact with T24 cells was 80% lower than the exponent of the controls (0.02 vs. 0.1, Table 2). Similarly, the exponent b of ECs in contact with T24 cells was also smaller (23% lower than that of the controls). In addition, G' of ECs in contact with T24 cells overall exhibited values lower than G' of the controls. Statistical analysis showed that the two curves were significantly different ($p < 0.0001$, F = 43.44 (4,22), Table 2). In contrast, for the viscous modulus G'', the F-test showed that there is a single curve that fits both the control and the ECs in-contact. There was no significant difference between these two distributions ($p = 0.07$, F = 2.54 (4.22), Table 2).
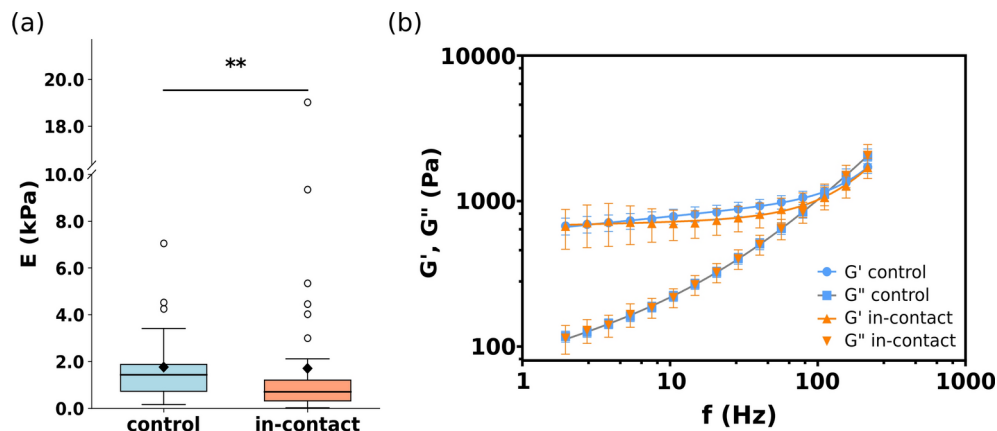
Fig. 2. Stiffness and viscoelastic moduli of ECs in contact with T24 cancer cells were decreased compared to the controls. (**a**) Boxplot of the Young's modulus E of the controls (blue, n =29) and ECs in contact with T24 cells (orange, n = 40) ($p < 0.01$, Mann–Whitney U test). (**b**) G' and G'' of controls (blue, n = 29) and ECs in contact with T24 cells (orange, n = 40) as a function of frequency. Data points correspond to the mean value, and error bars stand for the SEM. The continuous curves correspond to the best fittings of the data, according to Eq. (3). The fitting parameters are listed in Table 2.

	G_a (Pa)	a	G_b (Pa)	b	R^2	*p*-value	F-value
G'_{ctrl} (Pa)	618.1	0.1	0.009	2.07	0.999	<0.0001	43.44 (4,22)
G' (Pa)	674.4	0.02	0.17	1.6	0.996		
	G_c (Pa)	c	G_d (Pa)	d	R^2	*p*-value	F-value
G''_{ctrl} (Pa)	84.79	0.27	5.24	1.07	1	0.07	2.54 (4,22)
G'' (Pa)	84.87	0.26	5.05	1.08	1		

Table 2. Fitting parameters of G', G'' and their statistical comparison results (in-contact case).

As before, both moduli G' and G'' increased as a function of frequency. We observed that ECs in direct contact with T24 transitioned into a glassy state at a lower frequency (f_T = 99.5 Hz) than the control group (118.0 Hz).

Finally, comparing the relative changes in viscoelastic moduli, it can be concluded that the most significant difference is the slope a, undergoing a larger change with respect to the control (a going from 0.02 to 0.1) in the in-contact case as compared to the T24-ECGM case (a going from 0.07 to 0.09).

Actin distribution in endothelial cells cultured in T24-ECGM and in contact with T24 cancer cells

In order to complete the data on changes in the mechanical properties, we performed image analysis of the actin distribution within the ECs. Representative fluorescence images from two controls and two experimental cases are shown in Fig. 3a and d. The analysis was based on the thresholding of the pixels with gray values corresponding to the actin. For each image, the total actin area was measured and normalized to the effective area of the entire image. The number of images which was analyzed for each group was: T24-ECGM n = 42, corresponding Control n = 30; In-contact n = 40, corresponding Control n = 32. Two actin subtypes were distinguished during the analysis—visible fibers and larger clusters. Our study showed a significant decrease (p = 0.006) in the relative area of actin organized into clusters (mean $\frac{A_c}{A_e}$: T24-ECGM 0.119 ± 0.003 vs. control 0.133 ± 0.004) in endothelial cells cultured in the medium preconditioned by cancer cells, while the distribution of fibers was the same (mean $\frac{A_f}{A_e}$: 0.514 ± 0.010 in both groups, p = 0.97), see Fig. 3b,c. In the presence of physical contact of cancer cells with the endothelium, the observed changes had the same direction and were even more pronounced (Fig. 3e,f): mean $\frac{A_c}{A_e}$ in-contact 0.121 ± 0.004 versus control 0.131 ± 0.004 (p = 0.03) for the clusters case; mean $\frac{A_f}{A_e}$ in-contact 0.502 ± 0.013 vs. control 0.549 ± 0.007 for the fibers case (p = 0.009).

Discussion

While the interaction between endothelial cells and cancer cells has been a subject of previous research[7,11,35], the complete extent of this relationship remains largely unexplored. Using an AFM-based microrheology technique,
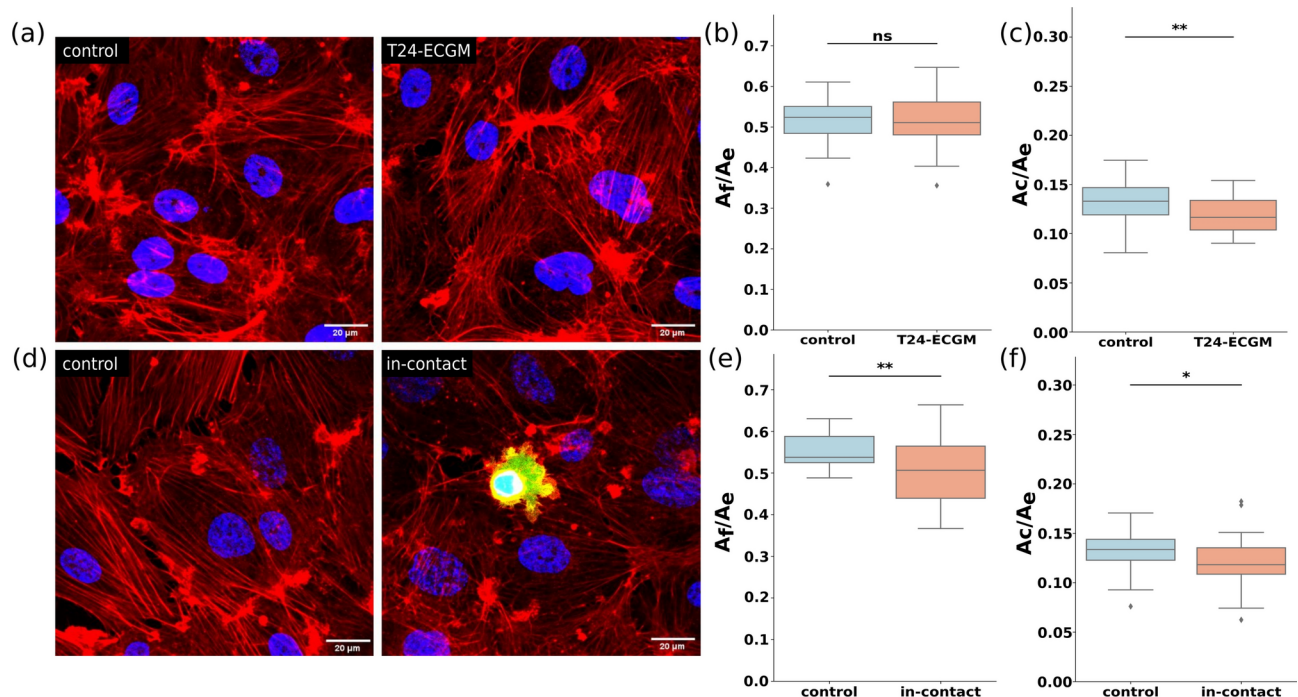
Fig. 3. Representative confocal images of endothelial cells. (**a**) Control ECs versus ECs cultured in T24-ECGM, (**d**) Control ECs vs. ECs in contact with cancer cells. Cells were stained to localize actin fibers (Phalloidin, red) and nuclei (Hoechst, blue). Actin–GFP transfected T24 cancer cells were used to localize the sites of contact with ECs (green). Normalized total area of actin fibers ($\frac{A_f}{A_e}$) and clusters ($\frac{A_c}{A_e}$) for ECs (**b, c**) cultured in T24-ECGM and (**e, f**) ECs in-contact with CCs. Scale bar = 20 μm.

we investigated the stiffness (E) and viscoelastic properties of endothelial cells in the presence of cancer cells or in medium enriched with paracrine CC factors (Fig. 5). Our results uncover previously unknown changes in the mechanical properties of endothelial cells under the influence of cancer cell-secreted substances, revealing new insights into the mechanisms of EC behaviour under cancer-related conditions. It is known that circulating tumour cells can remain in the bloodstream for a long time before extravasating and causing secondary tumour growth in a specific organ. To study whether tumour cells could affect the endothelium during this circulating stage without direct contact and attachment, we chose the following experimental strategy: when T24-ECGM medium was used (24 h), no tumour cells were present and any changes in the properties of ECs could be attributed to the molecules secreted by the T24 cancer cells. When T24 cells were added to ECs, the effect of intercellular contact prevailed, since fresh ECGM was used to prepare cancer cell suspension and the time of interaction was short (< 30 min).

Young's modulus (E) measurements showed the softening of ECs in the presence of cancer cell secreted substances. The stiffness of ECs cultured in T24-ECGM (median = 1.3 kPa) was lower than that of the corresponding controls (ECs in conventional ECGM, 1.8 kPa), although the difference was not significant (Fig. 1a). On the other hand, a significant decrease in their stiffness was observed when ECs were in direct contact with T24 cells, i.e. 0.7 kPa, versus 1.4 kPa for the controls (Fig. 2a). These results are in agreement with a previous study conducted by Mierke[31]. In this study, the author used magnetic tweezers to show that the stiffness of the ECs co-cultured with highly invasive cancer cells was decreased compared to the control sample. Abidine et al.[17] reported that the transmigration of a T24 cell through an endothelial monolayer occurs in approximately 20 min. Therefore, in contrast to the approach of Mierke[31], we were interested in the immediate influence of cancer cells on the stiffness of ECs. To evaluate the mechanics of ECs in this specific time window, we started our AFM-measurements immediately after the addition of T24 cells to the EC monolayer, and limited the period of measurement to the first 30 min. The consistent behaviour of ECs under both conditions (in T24-ECGM and in contact with T24 cells) demonstrated the very important role of secreted substances in driving the reduction in EC stiffness. However, it was found that the relative modulus $\frac{E}{E_{ctrl}}$ was significantly smaller (p < 0.05) for the contact case (0.51), as compared to the T24-ECGM (0.75), indicating a more important effect in the case of contact with T24 cells.

The microrheology study further confirmed that the viscoelastic properties of ECs were altered under the influence of cancer cells. The elastic modulus G' of ECs cultured in T24-ECGM was lower compared to the control sample (Fig. 1b), over the full frequency range studied, showing a similar trend to that observed for E. This supports the fact that the stiffness of ECs was reduced in the presence of substances secreted by cancer cells. The model exponents for G' (Eq. (3)) of ECs in T24-ECGM were significantly larger compared to controls (1.28

times larger for exponent a and 1.09 times larger for exponent b, for G', Table 1). Subsequently, the G' and G'' cross-over frequency f_T of ECs in T24-ECGM was larger than in controls, indicating a delay in the dominance of the viscous properties of ECs. Similarly, the G' of ECs in contact with T24 cells showed significantly lower values compared to the controls (Fig. 2b). Interestingly the slope a of G' was found much smaller in the case of contact with T24 cells, whereas it was rather similar when using the T24-ECGM medium. However, in this case, the fitting of the G'' data showed only one curve describing both the control and the ECs in-contact data points, indicating a non significant difference between the two data sets (Table 2). While the elasticity of ECs was altered, there were no changes in their viscous modulus due to their contact with cancer cells. The ECs showed an increasing stiffness as a function of frequency, in agreement with power-law regimes found in the literature data on cells[17,42,43] or epithelium layers[44]. These changes are attributed to modifications of the cell cytoskeleton, that can be described as a self-similar system with elements such as springs and dashpots organized at multiple levels[42]. At lower frequencies, the elastic modulus G' was larger than the viscous modulus G''. This is the frequency range of interest for transmigration of cancer cells through the endothelium, a phenomenon occurring at long timescales[17]. The cells had an elastic–like behaviour for frequencies below the cross-over frequency f_T, while they underwent a glassy transition at higher frequencies[45]. In this high-frequency regime, the deformations are so rapid that the cell cytoskeleton does not have enough time to relax, resulting in the emergence of a metastable (disordered) state[39,45–49]. In our study, the cross-over of the two moduli occurred at a lower frequency for ECs in direct contact with cancer cells, whereas the opposite was observed for ECs in T24-ECGM, i.e. a higher cross-over frequency compared to the controls. This result indicates the different time responses of ECs in these two conditions. A lower cross-over frequency for the in-contact case indicates a slower adaptation of these ECs to the mechanical stress, while ECs after 24 h of incubation in culture medium enriched with cancer cells-secreted substances showed faster mechanical response to stress. This could be due to structural changes in ECs under the influence of cancer signalling, resulting in a shorter timescale response to mechanical stress compared to slow rearrangements of the cytoskeleton of ECs in direct contact with T24. In our work, all curves were fitted with two power-laws as in Eq. (3). No universal power law has been found for cells[50], but the exponents a and c are typically in the range [0.1–0.3][42,51], while at higher frequencies exponents can become larger, as found in this work.

To investigate the cytoskeleton reorganization in ECs under these two experimental conditions, we performed fluorescence imaging of the actin cytoskeleton followed by image analysis. As typically shown in Fig. 3a and d, the cytoskeleton of ECs in T24-ECGM or in the presence of T24 cells underwent significant changes. Depending on the case considered, different features of actin cytoskeleton were observed. A segmentation technique (Fig. 6) was used to identify actin fibers or bigger clusters. The normalized total area of fibers and clusters was calculated (see Fig. 3b–f) in both cases. It appeared that in T24-ECGM or in the presence of T24 cells, the normalized total ratios of fibers $\frac{A_f}{A_e}$ and clusters $\frac{A_c}{A_e}$ always decreased as compared to the corresponding controls. This effect was always significant, except in the case of $\frac{A_f}{A_e}$ in T24-ECGM. Such reorganization of actin in clusters and fibers reflected changes in junctional and cytoplasmic network[52,53]. This finding is particularly relevant when compared with the results obtained earlier for the decrease of the static modulus E and the viscoelastic properties of ECs, as measured with AFM.

To understand these mechanisms further (Fig. 4), it is important to recall the process of extravasation, during which circulating cancer cells start with weak adhesion to the endothelium under blood flow and become stabilized by strong adhesion. It is known that selectins expressed on endothelial cells mediate such weak adhesion. Strong adhesion is mainly ensured by intercellular adhesion molecules located on the endothelium surface. ICAM-1 and VCAM-1 are constantly expressed at low levels on resting endothelium and are highly upregulated by inflammatory mediators[4,54]. In previous work, we showed that the expression of E-selectin, ICAM-1 and VCAM-1 on the surface of endothelial cells is upregulated after coculture with T24 cancer cells[11]. Cancer cell adhesion and clustering of ICAM-1 and VCAM-1 activates downstream signalling pathways, including recruitment of actin binding proteins (ABPs) that help coordinate actin remodelling[55]. Furthermore, direct contact between cancer cells and the endothelium (Fig. 4c) can activate the TGF-β signalling pathway, leading to disruption of intercellular adherens, for example VE-cadherins and PCAM-1[31], claudins, occludins[56], thus facilitating cancer cells transendothelial migration.

At the same time, paracrine factors secreted by CCs can affect endothelial cells, including inflammatory cytokines (TNF-α, IL-6, etc.)[37,38,57], growth factors (TGF-β)[58], miRNA and extracellular vesicles[35,59]. The long-term action of such a complex of factors can provoke some extent of endothelial to mesenchymal transition (EndMT),[58] accompanied by changes in endothelial properties, including altered cell polarity, weakening of cell–cell junctions and cytoskeleton remodelling to facilitate CCs transmigration through the endothelium[58,60]. Our results suggest that CCs secret substances that can influence the mechanical properties of ECs even in the absence of adhesion, prior to CCs attachment (Fig. 4a,b), thus making ECs softer in order to facilitate the transmigration process. In general, ECs tend to align along the direction of larger stresses[61], but disruptions in the force field can show possible misalignment of ECs[62]. On the other hand, HUVECs can change alignment when cultured in cancer cell medium[7]. Combining these studies, we suggest that cancer cell-secreted substances may induce the EC cytoskeleton rearrangement and alter the stress field prior to the complete attachment of CCs.

Taken together, our observations and results from the literature suggest that the process of endothelial cell softening, induced by cancer cells themselves or by their locally secreted factors, starts with the disruption of the cytoskeleton and adherens junctions (Fig. 4a–c) and could eventually lead to the formation of intercellular or, in some cases, intracellular gaps[64]. Therefore, this study advanced the knowledge of the role of cancer cell-secreted substances in altering the mechanical properties of the endothelium and creates opportunities for targeted future work on the transmigration of cancer cells across the endothelium.
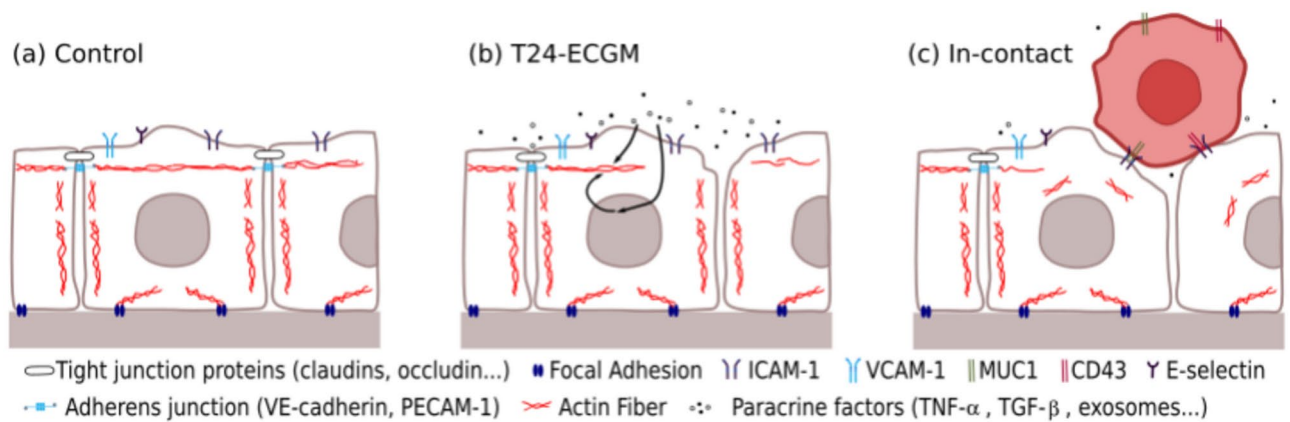
(a) Control (b) T24-ECGM (c) In-contact

◯ Tight junction proteins (claudins, occludin...) ■ Focal Adhesion)⊢ ICAM-1)⊢ VCAM-1 ‖ MUC1 ‖ CD43 Y E-selectin
·■· Adherens junction (VE-cadherin, PECAM-1) ✂ Actin Fiber ·:· Paracrine factors (TNF-α , TGF-β , exosomes...)

Fig. 4. Cytoskeleton reorganization of endothelial cells through paracrine signalling or by contact with cancer cell. (**a**) control endothelial cells: the integrity of the endothelium is ensured by the actin cytoskeleton network and intercellular junctions (clusters) that connect neighboring cells[53,63]. Some actin fibers cross the cytoplasm and some fibers connect with intercellular junctions[52]. (**b**) Under paracrine signalling, the intercellular junctions are disrupted and fibers disconnected from junctions[56]. (**c**) Physical contact between cancer cells and endothelial cells bring major modifications of the actin cytoskeleton[56].

Methods

Cell culture and preparation

Human Umbilical Vein Endothelial Cells (HUVECs, PromoCell) were cultured in supplemented Endothelial Cell Growth Medium (ECGM, PromoCell) at 37°C, 5% CO_2 and 95% humidity. Cells at passages 4–6 were used.

Human bladder carcinoma T24 cells[17] transfected with actin-GFP (Green Fluorescent Protein) were cultured in RPMI 1640 medium (Gibco) supplemented with 10% FBS (Fetal Bovine Serum, Gibco) and penicillin-streptomycin (Gibco) at 37 °C, 5% CO_2 and 95% humidity.

For the AFM measurements, glass coverslips (30 mm diameter) were glued (Norland Optical UV curing adhesive, NOA 61) at the bottom of TPP Petri dishes (Dutscher) to enable microscopic imaging. HUVECs were seeded on the dishes coated with collagen (50 μg/mL), and incubated for 3 days to reach confluency. Cancer cell conditioned medium (T24-ECGM) was prepared by culturing T24 cells in ECGM for 3 days. The conditioned medium was collected, filtered through a 40 μm–pore cell strainer, and diluted with unconditioned ECGM at a ratio of 1:10. The medium in dishes with cultured HUVECs was then replaced with the diluted T24–ECGM, less than 24 hbefore starting the measurements. For control dishes, the same volume of medium was replaced with fresh ECGM (see Fig. 5).

For the HUVEC–T24 contact experiments, 20,000 T24 cells in ECGM were added to the HUVEC monolayer. The same volume of fresh medium was added to control dishes. Measurements in a single dish did not exceed 30 min starting from the addition of T24 cells (Fig. 5).

Measurements were performed on control HUVECs on the same day, under the same exact conditions as HUVECs treated with T24-ECGM or in contact with T24 cells. To minimize the errors deriving from passage numbers, culture conditions and calibration of our experimental setup, measurements were compared with their corresponding controls.

AFM measurements

An Atomic Force Microscope (JPK, Berlin, Germany) was used, coupled with an inverted microscope (Zeiss, D1 model), equipped with phase contrast and fluorescence. Experiments were performed at 37 °C. For each experiment, a cantilever with a pyramidal tip (MLCT-C, Bruker) was used. Cantilevers were calibrated (k ∼ 0.017 N/m) using the thermal noise method[65].

To investigate the cell properties, we used a microrheology AFM-based technique[40]. The cantilever was used to indent cells with an initial indentation δ_0 corresponding to an initial force setpoint $F_0 = 0.5$ nN. After the initial indentation, the height of the cantilever was kept constant and a small oscillatory displacement $\delta \sim 0.1\,\delta_0$ was superimposed to δ_0. Frequencies (*f*) in the range of 2–200 Hz were used for the oscillations. Measurements were performed on top of the cell nuclei. This choice is motivated by the fact that this region is flat and easy to indent, as compared to the cytoplasm or thin junctions. In addition, the fact that T24 cells interact at the junctions would make it difficult to measure at these locations. The Young's modulus E was obtained from the initial indentation, after adapting the Hertz formula, using correction effects due to small cell thickness[66]. Endothelial cells seeded on a glass coverslip are a few microns thick, so when indentations become too large, ECs may appear stiffer due to the hard substrate. Therefore the working Hertz formula was corrected as:

$$F_0 = \frac{3E \tan\theta\, \delta_0^2}{4(1-\nu^2)}\, g_B(\delta_0, h) \qquad (1)$$
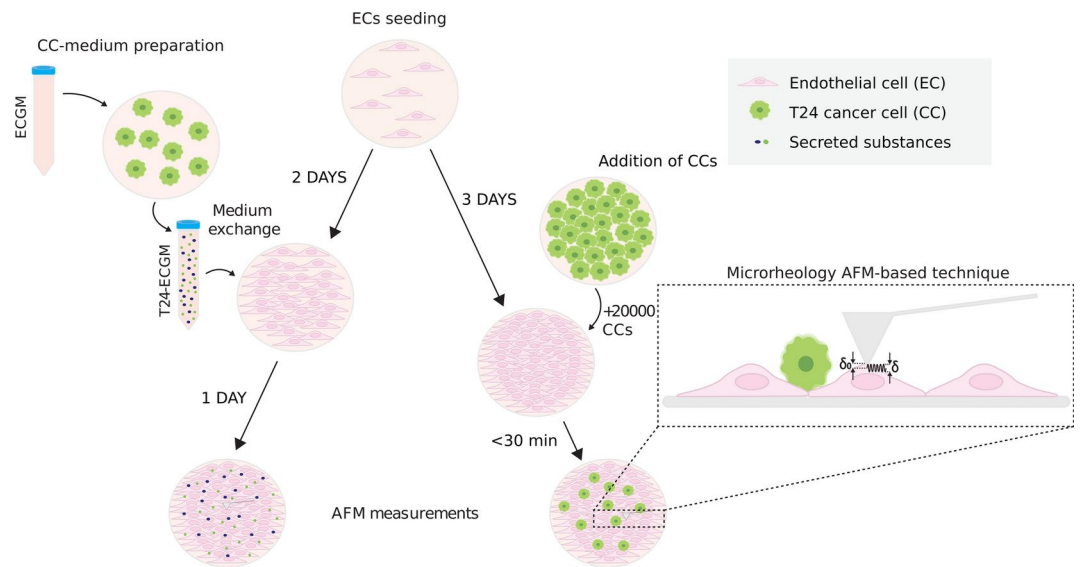
Fig. 5. Sketch of the experimental process. EC monolayers were studied using AFM under two different conditions: (1) culture of ECs in cancer cell conditioned medium for 1 day and (2) direct addition of cancer cells on the monolayer, with the measurements taking place within the first 30 min.

where F_0 is the force of the cantilever on the cell surface, ν is the cell's Poisson ratio (typically 0.5 for cells), θ is the half angle of the pyramidal tip ($\theta = 19°$), $g_B(\delta_0, h) = 1 + 0.6298\chi_0 + 0.7236\chi_0^2 + 1.249\chi_0^3 - 0.3556\chi_0^4$ and $\chi_0 = \frac{\delta_0 \tan \theta}{h}$, with h the cell height[66]. For measuring h, a force-displacement curve was taken first on the coverslip, then another one on the cell, just above the nucleus, using only the piezo movement, in order to achieve higher accuracy (~ 20 nm). A small force setpoint was chosen (0.1 nN) not to damage the cell. Comparing the two curves enabled to obtain the two contact points, and their difference provided the value of h.

When carrying small oscillations at frequency f, Eq. (1) was linearized as previously described[67]. Fourier transforms were taken for the force $F^* = Fe^{i\omega t}$ and displacement $\delta^* = \delta e^{i(\omega t + \phi)}$, with ω ($=2\pi f$) and ϕ the respective angular frequency and phase. Finally, using $E^* = 2G^*(1 + \nu)$, the final complex shear modulus became:

$$G^* = G' + i\,G'' = \frac{1 - \nu}{3\,\delta_0 \tan \theta} \frac{F^*}{\delta^*} g(\chi_0)^{-1} \tag{2}$$

where $g(\chi_0) = 1 + 0.945\chi_0 + 1.447\chi_0^2 + 3.108\chi_0^3 - 1.0068\chi_0^4$, and the hydrodynamic drag was substracted[17,68]. G' and G'' were respectively the elastic and loss shear cell moduli.

Rheological modeling

AFM measurements were performed on ECs cultured in T24-ECGM, or in contact with T24 cells, and in corresponding controls. For each cell, the Young's modulus was calculated from the initial approach of the cantilever on the cell, using Eq. (1).

The term g was the correction factor given above. Since the cells were rather thin ($h_{HUVEC} = 2.51 \pm 0.16\ \mu$m), the correction factor was necessary to correct for any effects caused by the hard substrate. The moduli G' and G'' from Eq. (2) were calculated at each frequency, for each cell. The data (G', G'') were then averaged over all experiments and plotted as a function of frequency. As for error bars, the Standard Error of the Mean (SEM) was used. When plotting G' and G'' as a function of frequency, the curves were fitted with a model similar to previous ones using power laws[50,67]:

$$G'(\omega) = G_a\,(\omega/\omega_0)^a + G_b\,(\omega/\omega_0)^b, \quad G''(\omega) = G_c\,(\omega/\omega_0)^c + G_d\,(\omega/\omega_0)^d \tag{3}$$

where $\omega_0 = 2\pi f_0$ (in s^{-1}) is a typical angular frequency (here we use f_0=1 Hz). G_a, G_b, G_c and G_d are adjustable moduli (in Pa), and a, b, c, d are exponents to be determined.

Image acquisition and processing

For visualization of the actin network of ECs, we performed immunostaining on all three conditions. The cells were fixed with 4% formaldehyde fixative solution (Invitrogen) and were stained for with Phalloidin TRITC (Sigma-Aldrich) for F-actin and with Hoechst 33342 (Invitrogen) for nuclear visualization. The dyes were used according to the manufacturer's specifications. Three samples were prepared for each of the two control groups and four for each of the two experimental groups (T24-ECGM and in-contact). Confocal fluorescence microscopy was performed on an inverted Leica TCS SP8 microscope, with a 40X/NA1.3 oil immersion objective. Three-dimensional image stacks were acquired, with a Z-slice spacing of 0.35 μm and a numerical zoom of 2, from 10
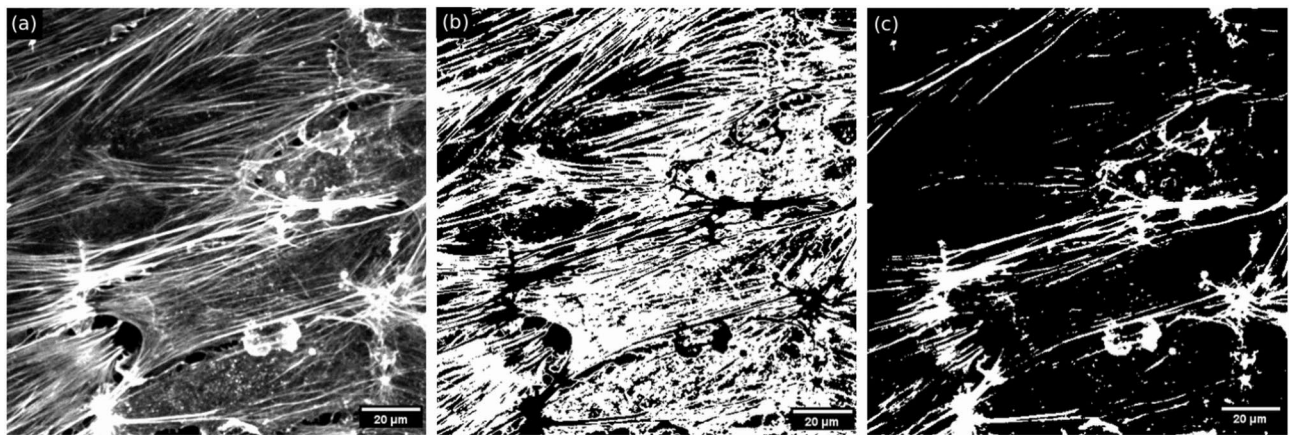
Fig. 6. Image processing for characterization of actin distribution in cells. (**a**) Z–projection of an image stack. (**b**) Binary mask for visible actin fibers and (**c**) for larger fiber clusters.

randomly selected fields of view per sample. Image stacks were processed and analyzed using the open-source ImageJ platform and built-in plugins[1].

To characterize the distribution of F-actin fibers within the cells, we visually distinguished two subtypes, visible fibers and fiber clusters. Z-projections of image stacks corresponding to F-actin staining were generated by averaging the intensity of the sections spanning the ECs monolayer (Fig. 6a). From each averaged image, two binary masks were created using the built-in 'Threshold option' - one for visible actin fibers (Fig. 6b) and the other for larger fiber clusters (Fig. 6c). A cutoff value between two thresholds was chosen individually for each image analyzed, based on the gray values histogram (with x-axis representing possible gray values and y-axis being the number of pixels for each gray value). Since 8–bit images were analyzed, the gray values range was 0–255. For each averaged image, the number of pixels corresponding to each possible gray value was normalized to the maximum number found. This transformation allowed to represent all the histograms on the same y-axis with a maximum $y_{max} = 1.0$ and to implement the same threshold ranges selection algorithm for all the images. Only the pixels with a gray value higher ($x_{max} < x$) than the revealed maxima were included in the thresholding. Threshold ranges were selected as follows (i) for fibers, gray values with normalized number of pixels $0.2 \leq y < 1$, and (ii) for fiber clusters, gray values with normalized number of pixels $y < 0.2$. From the generated binary masks, the total area covered by actin fibers (A_f) or fiber clusters (A_c) was measured using the 'Analyze Particles' option with a specified circularity range of 0–0.5. Considering that the endothelial cells were not at 100% confluency, to properly adjust the experimental conditions for AFM measurements, the cell-free area was rather important in some images. Therefore, for each image, the cell-free area was subtracted from the total image area, to provide the effective area (A_e), and the actin data was presented as the ratio of actin area over this effective area: $\frac{A_f}{A_e}$ or $\frac{A_c}{A_e}$. For the in–contact group, only ECs in direct physical contact with T24 cancer cells were included in the analysis.

Statistical analysis

Data processing was performed using a custom-written program in python. The data were plotted and tested for significance using GraphPrism and python. The data sets plotted in boxplots were tested for normality using the Shapiro-Wilcoxon test and for similar variance using F-test. T-test and Mann-Whitney U tests were used accordingly. The horizontal line corresponds to the median, while the filled rhombus shows the mean of the datasets. Two data distributions were considered to be significantly different when the p value was lower than a given value: $p < 0.05$ *, $p < 0.01$ **, $p < 0.001$ ***. For the XY-plots, the averaged data points were plotted, with the corresponding Standard Error of the Mean (SEM). The fits were tested for significance using the extra-sum-of-squares F-test. The F-value is given, along with its two degrees of freedom in parenthesis (F-value (df1,df2)). The two fits were significantly different when the F-value was larger than the corresponding value in the F-distribution table, according to the specific degrees of freedom.

Data availability

The datasets used and analysed during the current study are available from the corresponding author on reasonable request.

---

[1] Rasband, WS, ImageJ, US National Institutes of Health, Bethesda, Maryland, USA, https://imagej.net/ij/, 1997-2018

References

1. Sturtzel, C. Endothelial cells. In *The Immunology of Cardiovascular Homeostasis and Pathology* (eds Sattler, S. & Kennedy-Lydon, T.) 71–9 (Springer, 2017). https://doi.org/10.1007/978-3-319-57613-8_4.
2. Stanek, A., Fazeli, B., Bartuś, S. & Sutkowska, E. The role of endothelium in physiological and pathological states: New data. *Biomed. Res. Int.* **2018**, 1098039. https://doi.org/10.1155/2018/1098039 (2018).
3. Liu, Z., Sniadecki, N. J. & Chen, C. S. Mechanical forces in endothelial cells during firm adhesion and early transmigration of human monocytes. *Cell. Mol. Bioeng.* **3**, 50–59. https://doi.org/10.1007/s12195-010-0105-3 (2010).
4. van Steen, A. C., van der Meer, W. J., Hoefer, I. E. & van Buul, J. D. Actin remodelling of the endothelium during transendothelial migration of leukocytes. *Atherosclerosis* **315**, 102–110. https://doi.org/10.1016/j.atherosclerosis.2020.06.004 (2020).
5. Lin, D. et al. Circulating tumor cells: Biology and clinical significance. *Sig. Transduct. Target. Ther.* **6**, 404. https://doi.org/10.1038/s41392-021-00817-8 (2021).
6. Mierke, C. Endothelial cell's biomechanical properties are regulated by invasive cancer cells. *Mol. Bioyst.* **8**, 1639–49. https://doi.org/10.1039/c2mb25024a (2012).
7. Hang, B. et al. Interacting with tumor cells weakens the intrinsic clockwise chirality of endothelial cells. *APL Bioeng.* **6**, 2473–2877. https://doi.org/10.1063/5.0115827 (2022).
8. Reymond, N. et al. Cdc42 promotes transendothelial migration of cancer cells through β1 integrin. *J. Cell Biol.* **199**, 653–668. https://doi.org/10.1083/jcb.201205169 (2012).
9. Chen, M. B., Lamar, J. M., Li, R., Hynes, R. O. & Kamm, R. D. Elucidation of the roles of tumor integrin ß1 in the extravasation stage of the metastasis cascade. *Cancer Res.* **76**, 2513–2524. https://doi.org/10.1158/0008-5472.CAN-15-1325 (2016).
10. Sundar Rajan, V., Laurent, V. M., Verdier, C. & Duperray, A. Unraveling the Receptor-Ligand Interactions between bladder cancer cells and the endothelium using AFM. *Biophys. J.* **112**, 1246–1257. https://doi.org/10.1016/j.bpj.2017.01.033 (2017).
11. Haddad, O., Chotard-Ghodsnia, R., Verdier, C. & Duperray, A. Tumor cell/endothelial cell tight contact upregulates endothelial adhesion molecule expression mediated by nfκb: Differential role of the shear stress. *Exp. Cell Res.* **316**, 615–626. https://doi.org/10.1016/j.yexcr.2009.11.015 (2010).
12. Laurent, V. M., Duperray, A., Sundar Rajan, V. E. J. & Verdier, C. Atomic force microscopy reveals a role for endothelial cell icam-1 expression in bladder cancer cell adherence. *PLoS ONE* **9**, e98034. https://doi.org/10.1371/journal.pone.0098034 (2014).
13. Laferriere, J., Houle, F., Taher, M. M., Valerie, K. & Huot, J. Transendothelial migration of colon carcinoma cells requires expression of e-selectin by endothelial cells and activation of stress-activated protein kinase-2 (SAPK2/p38) in the tumor cells. *J. Biol. Chem.* **276**, 33762–33772. https://doi.org/10.1074/jbc.M008564200 (2001).
14. Shenoy, A. K. & Lu, J. Cancer cells remodel themselves and vasculature to overcome the endothelial barrier. *Cancer Lett.* **380**, 534–544. https://doi.org/10.1016/j.canlet.2014.10.031 (2014).
15. Lekka, M. Discrimination between normal and cancerous cells using AFM. *Bionanoscience* **6**, 65–80. https://doi.org/10.1007/s12668-016-0191-3 (2016).
16. Molnár, J. et al. Transmigration characteristics of breast cancer and melanoma cells through the brain endothelium: Role of RAC and PI3K. *Cell Adhes. Migr.* **10**, 269–281. https://doi.org/10.1080/19336918.2015.1122156 (2016).
17. Abidine, Y. et al. Mechanosensitivity of cancer cells in contact with soft substrates using AFM. *Biophys. J*. **114**, 1165–1175. https://doi.org/10.1016/j.bpj.2018.01.005 (2018).
18. Arefi, S. M. A., Tsvirkun, D., Verdier, C. & Feng, J. J. A biomechanical model for the transendothelial migration of cancer cells. *Phys. Biol.* **17**, 036004. https://doi.org/10.1088/1478-3975/ab725c (2020).
19. Javanmardi, Y. et al. Endothelium and subendothelial matrix mechanics modulate cancer cell transendothelial migration. *Adv. Sci.* https://doi.org/10.1002/advs.202206554 (2023).
20. Heyder, C. et al. Realtime visualization of tumor cell/endothelial cell interactions during transmigration across the endothelial barrier. *J. Cancer Res. Clin. Oncol.* **128**, 533–538. https://doi.org/10.1007/s00432-002-0377-7 (2002).
21. Chen, M. B., Whisler, J. A., Jeon, J. S. & Kamm, R. D. Mechanisms of tumor cell extravasation in an in vitro microvascular network platform. *Integr. Biol.* **5**, 1262–1271. https://doi.org/10.1039/c3ib40149a (2013).
22. Jeon, J. S., Zervantonakis, I. K., Chung, S., Kamm, R. D. & Charest, J. L. In vitro model of tumor cell extravasation. *PLoS ONE* **8**, e56910. https://doi.org/10.1371/journal.pone.0056910 (2013).
23. Aragon-Sanabria, V. et al. VE-cadherin disassembly and cell contractility in the endothelium are necessary for barrier disruption induced by tumor cells. *Sci. Rep.* **7**, 45835. https://doi.org/10.1038/srep45835 (2017).
24. Brock, T. et al. The influence of VE-cadherin on adhesion and incorporation of breast cancer cells into vascular endothelium. *Int. J. Mol. Sci.* **22**, 6049. https://doi.org/10.3390/ijms22116049 (2021).
25. Qi, J., Chen, N., Wang, J. & Siu, C.-H. Transendothelial migration of melanoma cells involves N-cadherin-mediated adhesion and activation of the beta-catenin signaling pathway. *Mol. Biol. Cell* **16**, 4386–4397. https://doi.org/10.1091/mbc.E05-03-0186 (2005).
26. Weidert, E., Pohler, S. E., Gomez, E. W. & Dong, C. Actinomyosin contraction, phosphorylation of VE-cadherin, and actin remodeling enable melanoma-induced endothelial cell-cell junction disassembly. *PLoS ONE* **9**, e108092. https://doi.org/10.1371/journal.pone.0108092 (2014).
27. Grady, M. E., Composto, R. J. & Eckmann, D. M. Cell elasticity with altered cytoskeletal architectures across multiple cell types. *J. Mech. Behav. Biomed. Mater.* **61**, 197–207. https://doi.org/10.1016/j.jmbbm.2016.01.022 (2016).
28. Xie, L. et al. Changes in dynamics of tumor/endothelial cell adhesive interactions depending on endothelial cell growth state and elastic properties. *PLoS ONE* **17**, e0269552. https://doi.org/10.1371/journal.pone.0269552 (2022).
29. Wang, L., Tian, L., Zhang, W., Wang, Z. & Liu, X. Effect of AFM nanoindentation loading rate on the characterization of mechanical properties of vascular endothelial cel. *Micromachines* **11**, 562. https://doi.org/10.3390/mi11060562 (2020).
30. Starodubtseva, M. N. et al. Heterogeneity of nanomechanical properties of the human umbilical vein endothelial cell surface. *Microvasc. Res.* **136**, 104168. https://doi.org/10.1016/j.mvr.2021.104168 (2021).
31. Mierke, C. T. Cancer cells regulate biomechanical properties of human microvascular endothelial cells. *J. Biol. Chem.* **286**, 40025–40037. https://doi.org/10.1074/jbc.M111.256172 (2011).
32. Arce, F. T. et al. Lamellipodia dynamics and microrheology in endothelial cell paracellular gap closure. *Biophys. J*. **122**, 4730–4747. https://doi.org/10.1038/srep4583 (2023).
33. Zhang, N., Hao, J., Cai, Y. & Wang, M. Research advances of secretory proteins in malignant tumors. *Chin. J. Cancer Res.* **33**, 115–132. https://doi.org/10.21147/j.issn.1000-9604.2021.01.12 (2021).
34. Griffith, L. G. & Swartz, M. A. Capturing complex 3D tissue physiology in vitro. *Nat. Rev. Mol. Cell Bio.* **7**, 211–224. https://doi.org/10.1038/nrm1858 (2006).
35. Cen, J. et al. Exosomal thrombospondin-1 disrupts the integrity of endothelial intercellular junctions to facilitate breast cancer cell metastasis. *Cancers* https://doi.org/10.3390/cancers11121946 (2019).
36. Cho, J. G., Lee, A., Chang, W., Lee, M.-S. & Kim, J. Endothelial to mesenchymal transition represents a key link in the interaction between inflammation and endothelial dysfunction. *Front. Immunol.* **9**, 294. https://doi.org/10.3389/fimmu.2018.00294 (2018).
37. Li, R., Wen, A. & Lin, J. Pro-inflammatory cytokines in the formation of the pre-metastatic niche. *Cancers* **12**, 3752. https://doi.org/10.3390/cancers12123752 (2020).
38. Aguilar-Cazares, D. et al. The systemic-level repercussions of cancer-associated inflammation mediators produced in the tumor microenvironment. *Front. Endocrinol.* https://doi.org/10.3389/fendo.2022.929572 (2022).
39. Mahaffy, R. E., Park, S., Gerde, E., Käs, J. & Shih, C. K. Quantitative analysis of the viscoelastic properties of thin regions of fibroblasts using atomic force microscopy. *Biophys. J*. **86**, 1777–1793. https://doi.org/10.1016/S0006-3495(04)74245-9 (2004).

10

40. Alcaraz, J. et al. Microrheology of human lung epithelial cells measured by atomic force microscopy. *Biophys. J*. **84**, 2071–2079. https://doi.org/10.1016/S0006-3495(03)75014-0 (2003).
41. Lherbette, M. et al. Atomic force microscopy micro-rheology reveals large structural inhomogeneities in single cell-nuclei. *Sci. Rep.* **7**, 8116. https://doi.org/10.1038/s41598-017-08517-6 (2017).
42. Hang, J.-T., Xu, G.-K. & Gao, H. Frequency-dependent transition in power-law rheological behavior of living cells. *Sci. Adv.* https://doi.org/10.1126/sciadv.abn6093 (2022).
43. Rebêlo, L. M. et al. Microrheology of cells with magnetic force modulation atomic force microscopy. *Soft Matter* **10**, 2141–2149. https://doi.org/10.1039/C3SM52045E (2014).
44. Wang, H., Liu, Y.-Q., Hang, J.-T., Xu, G.-K. & Feng, X.-Q. Dynamic high-order buckling and spontaneous recovery of active epithelial tissues. *J. Mech. Phys. Solids* **183**, 105496. https://doi.org/10.1016/j.jmps.2023.105496 (2024).
45. Abidine, Y. et al. Physical properties of polyacrylamide gels probed by AFM and rheology. *Europhys. Lett.* **109**, 38003. https://doi.org/10.1209/0295-5075/109/38003 (2015).
46. Fabry, B. et al. Scaling the microrheology of living cells. *Phys. Rev. Lett.* **87**, 148102. https://doi.org/10.1103/PhysRevLett.87.148102 (2001).
47. Rother, J., Nöding, H., Mey, I. & Janshoff, A. Atomic force microscopy-based microrheology reveals significant differences in the viscoelastic response between malign and benign cell lines. *Open Biol.* **4**, 140046. https://doi.org/10.1098/rsob.140046 (2014).
48. Rigato, A., Miyagi, A., Scheuring, S. & Rico, F. High-frequency microrheology reveals cytoskeleton dynamics in living cells. *Nat. Phys.* **13**, 771–775. https://doi.org/10.1038/nphys4104 (2017).
49. Flormann, D. A. D. et al. Oscillatory microrheology, creep compliance and stress relaxation of biological cells reveal strong correlations as probed by atomic force microscopy. *Front. Phys.* https://doi.org/10.3389/fphy.2021.711860 (2021).
50. Stamenovic, D. et al. Rheological behavior of living cells is timescale-dependent. *Biophys. J*. **93**, L39–L41. https://doi.org/10.1529/biophysj.107.116582 (2007).
51. Deng, L. et al. Fast and slow dynamics of the cytoskeleton. *Nat. Mater.* **5**, 636–640. https://doi.org/10.1038/nmat1685 (2006).
52. van Geemen, D. et al. F-actin-anchored focal adhesions distinguish endothelial phenotypes of human arteries and veins. *Arterioscler. Thromb. Vasc. Biol.* **34**(9), 2059–2067. https://doi.org/10.1161/ATVBAHA.114.304180 (2014).
53. Cronin, N. & DeMali, K. Dynamics of the actin cytoskeleton at adhesion complexes. *Biology* **11**, 1–12. https://doi.org/10.3390/biology11010052 (2021).
54. van Buul, J. D. et al. ICAM-1 clustering on endothelial cells recruits VCAM-1. *J. Biomed. Biotechnol.* **2010**, 1–9. https://doi.org/10.1155/2010/120328 (2010).
55. García-Ponce, A., Citalán-Madrid, A. F., Velázquez-Avila, M., Vargas-Robles, H. & Schnoor, M. The role of actin-binding proteins in the control of endothelial barrier integrity. *Thromb. Haemostasis* **113**, 20–36. https://doi.org/10.1160/th14-04-0298 (2015).
56. Gasparics, Á., Rosivall, L., Krizbai, I. A. & Sebe, A. When the endothelium scores an own goal: endothelial cells actively augment metastatic extravasation through endothelial-mesenchymal transition. *Am. J. Physiol. Heart Circ. Physiol.* **310**(9), H1055–H1063. https://doi.org/10.1152/ajpheart.00042.2016 (2016).
57. Kartikasari, A. E. R., Huertas, C. S., Mitchell, A. & Plebanski, M. Tumor-induced inflammatory cytokines and the emerging diagnostic devices for cancer detection and prognosis. *Front. Oncol.* https://doi.org/10.3389/fonc.2021.692142 (2021).
58. Ma, J., Sanchez-Duffhues, G., Goumans, M.-J. & ten Dijke, P. TGF-beta-induced endothelial to mesenchymal transition in disease and tissue engineering. *Front. Cell Dev. Biol.* https://doi.org/10.3389/fcell.2020.00260 (2020).
59. Liu, Z., Du, D. & Zhang, S. Tumor-derived exosomal mir-1247-3p promotes angiogenesis in bladder cancer by targeting FOXO1. *Cancer Biol. Therapy* https://doi.org/10.1080/15384047.2023.2290033 (2023).
60. Leggett, S. E., Hruska, A. M., Guo, M. & Wong, I. Y. The epithelial-mesenchymal transition and the cytoskeleton in bioengineered systems. *Cell Commun. Signal.* https://doi.org/10.1186/s12964-021-00713-2 (2021).
61. Liu, C., He, S., Li, X. & Huo, B. Mechanics of cell mechanosensing on patterned substrate. *J. Appl. Mech.* **83**, 051014. https://doi.org/10.1115/1.4032907 (2016).
62. Cui, X. et al. Mechanical forces regulate asymmetric vascular cell alignment. *Biophys. J*. **119**, 1771–1780. https://doi.org/10.1016/j.bpj.2020.09.020 (2020).
63. Prasain, N. & Stevens, T. The actin cytoskeleton in endothelial cell phenotypes. *Microvasc. Res.* **77**(1), 53–63. https://doi.org/10.1016/j.mvr.2008.09.012 (2009).
64. Ebben, A. & Dabagh, M. Mechanotransduction in endothelial cells in vicinity of cancer cells. *Cell. Mol. Bioeng.* **15**, 313–330. https://doi.org/10.1007/s12195-022-00728-w (2022).
65. Hutter, J. L. & Bechhoefer, J. Calibration of atomic-force microscope tips. *Rev. Sci. Instrum.* **64**, 1868–1873. https://doi.org/10.1063/1.1143970 (1993).
66. Santos, J. A. C., Rebêlo, L. M., Araujo, A. C., Barros, E. B. & de Sousa, J. S. Thickness-corrected model for nanoindentation of thin films with conical indenters. *Soft Matter* **8**, 4441–4448. https://doi.org/10.1039/C2SM07062F (2012).
67. Abidine, Y., Laurent, V. M., Michel, R., Duperray, A. & Verdier, C. Local mechanical properties of bladder cancer cells measured by AFM as a signature of metastatic potential. *Eur. J. Phys. Plus* **130**, 202. https://doi.org/10.1140/epjp/i2015-15202-6 (2015).
68. Alcaraz, J. et al. Correction of microrheological measurements of soft samples with atomic force microscopy for the hydrodynamic drag on the cantilever. *Langmuir* **18**, 716–721. https://doi.org/10.1021/la011085 (2002).

Acknowledgements

Author contributions

G.M.K. carried out AFM experiments and data analysis. D.T. helped with cell culture and carried out confocal experiments and image analysis. C.V. and V.M.L. helped with AFM experiments and data analysis. D.T., V.M.L. and C.V. designed research. All authors contributed to the writing, editing and discussing the article.

Declarations

Competing interests

The authors declare no competing interests.

Additional information

Correspondence and requests for materials should be addressed to C.V.

Reprints and permissions information is available at www.nature.com/reprints.

Publisher's note Springer Nature remains neutral with regard to jurisdictional claims in published maps and institutional affiliations.